International Journal of Refrigeration 104 (2019) 367–375

Contents lists available at ScienceDirect

International Journal of Refrigeration

journal homepage: www.elsevier.com/locate/ijrefrig

Effect of plates coating on performance of an indirect evaporative cooling system

Manfredo Guilizzoni[a], Samanta Milani[a], Paolo Liberati[b], Stefano De Antonellis[a,*]

[a] Dipartimento di Energia, Politecnico di Milano, Via Lambruschini 4, 20156 Milan, Italy
[b] Recuperator S.p.A., Via Valfurva 13, 20027 Rescaldina MI, Italy

ARTICLE INFO

Article history:
Received 30 November 2018
Revised 17 April 2019
Accepted 20 May 2019
Available online 23 May 2019

Keywords:
Indirect Evaporative Cooler
IEC
Wettability
Hydrophilic
Experimental

ABSTRACT

In this paper an experimental analysis of two different indirect evaporative cooling (IEC) systems is carried out: in the first one plates heat exchanger are finished with a standard epoxy coating (STD) while in the second one a novel hydrophilic lacquer is adopted (HPHI). Firstly, static contact angles, water retention and transient drop-surface interaction of both materials are evaluated. Secondly, IEC systems performance is measured in different operating conditions and, in particular, varying the water flowrate and nozzle position (top and side).

Results highlight that contact angles of HPHI coating are always lower than the ones of STD treatment: according to these findings, in case of water distribution from the top of the IEC system, wet bulb effectiveness of HPHI device is higher than that of STD unit (up to 10%). Instead, in case of water flow supplied from the side of the system, no significant differences have been observed.

Effet de l'enrobage des plaques sur les performances d'un système de refroidissement évaporatif indirect

Mots-clés: Refroidisseur évaporatif indirect (IEC); IEC; Mouillabilité; Hydrophile; Expérimental

1. Introduction

High-density data centers are energy intensive infrastructures: in 2010 they accounted for 1.1% - 1.5% of worldwide electricity use, doubling from 2000 to 2005 and increasing by about 56% from 2005 to 2010 (Koomey, 2011). The worldwide electricity consumption of data centers has been estimated around 270 TWh in 2012 and it is expected to increase in the next years due to the growth of IT services (Van Heddeghem et al., 2014).

Because of high heat fluxes dissipated by IT equipment, energy use of cooling devices is particularly relevant: electricity consumption of such systems has been evaluated around 40% of total energy consumption, with peaks even around 60% (Salim and Tozer, 2010). Therefore, improving the cooling process of the facility is a key issue that should be addressed in the next years to achieve significant energy savings in data centers.

At present, there is a great interest in the use of indirect evaporative cooling (IEC) systems in IT facilities. In fact, since the revision of the thermal guidelines for data processing environment by ASHRAE (ASHRAE 2008), the allowed indoor temperature and humidity ranges have been expanded, promoting the use of the aforementioned cooling technology. IEC systems are already effectively used in several applications, such as energy recovery units (Duan et al., 2012), power production (Najjar and Abubaker, 2015) or in desiccant/evaporative cooling open cycles (Chung and Lee, 2011; Goldsworthy and White, 2011).

In an indirect evaporative cooler, two airflows enter the system, denoted as the primary air and the secondary air streams. The primary air, which is supplied to the data center, flows along the dry channels of the heat exchanger. Instead, the secondary air is put in direct contact with water that flows in the wet channels of the system. Water evaporation leads to the cooling of the secondary airstream, and, due to the heat transfer across heat exchanger plates, of the primary airflow, whose humidity ratio keeps constant.

* Corresponding author.
E-mail address: stefano.deantonellis@polimi.it (S. De Antonellis).

https://doi.org/10.1016/j.ijrefrig.2019.05.029
0140-7007/

Nomenclature

A - E	experimental tests in wet conditions
cp	specific heat (kJ kg^{-1} K^{-1})
f_{eva}	fraction of evaporated water (-)
h	channel height (m)
L	net plates length and width (m)
$\dot{M}$	mass flow rate (kg s^{-1})
N_{HE}	mumber of plates (-)
pt	plates pitch (mm)
$\dot{Q}$	volumetric flow rate (m^3 h^{-1})
RH	relative humidity (-)
T	dry bulb temperature (°C)
T_{wb}	wet bulb temperature (°C)
u	experimental uncertainty
x_i	generic measured quantity (-)
X	humidity ratio (kg kg^{-1})
y_i	generic calculated quantity (-)
Greek letters	
δ	plates thickness (m)
ε_{db}	dry bulb effectiveness (-)
ε_{wb}	wet bulb effectiveness (-)
θ	contact angle (°)
σ	variance
Superscripts	
N	reference condition ($\rho = 1.2$ kg m^{-3})
Subscripts	
a	air
eva	evaporated water
in	inlet
inst	instrumental
min	minimum
net	net
out	outlet
p	primary air stream
s	secondary air stream
w	water
x_i	generic measured quantity
$\bar{x_i}$	mean of generic measured quantity
y_i	generic calculate quantity
Acronyms	
ADSA	Axisymmetric Drop Shape Analysis technique
ADSA-P	Axisymmetric Drop Shape Analysis technique - Profile
HPHI	HydroPHIlic coating/device
IEC	Indirect Evaporative Cooling/Cooler
MAD	Mean Absolute Deviation
SIDE	SIDE configuration
STD	STanDard (epoxy) coating/device
TOP	TOP configuration

Performance of the indirect evaporative cooling system is significantly related to water layer formation on heat exchanger plates, as discussed through numerical and experimental analysis in several scientific papers. Research studies highlighted that higher plates wettability remarkably enhances the indirect evaporative cooler performance (Guo and Zhao, 1998; Chengqin and Hongxing, 2006; Chua et al., 2016; De Antonellis et al., 2016; De Antonellis et al., 2017). The increase in the surface wettability factor, namely the wet to total area ratio, can be obtained mainly by: i) increasing the water flow rate (De Antonellis et al., 2016; De Antonellis et al., 2017), ii) using innovative materials or coatings (Zao et al., 2018; Lee and Lee, 2013); iii) adopting a proper system orientation (Li et al., 2018).

Several studies investigate the effect of different materials used to realize heat exchanger plates, in order to foster the wetting of the surface and the water evaporation (Zao et al., 2018; Wang et al., 2017; Xu et al., 2016; Xu et al., 2017; Lee and Lee, 2013). In particular, Zao et al. (2018) examined several types of substances to be used in IEC systems, suggesting a wick attained material (copper or aluminum) to promote heat and mass transfer. Wang et al. evaluated performance of a novel porous ceramic tube type indirect evaporative cooler and highlighted that the use of a hydrophilic coating leads to significant improvement of performance compared to conventional configurations (Wang et al., 2017). Xu et al. analyzed seven textile fabrics for IEC applications, concluding that some investigated samples have a great potential to increase system effectiveness (Xu et al., 2016). They also evaluated the performance of an innovative prototype (Xu et al., 2017) with plates made of aluminum alloy and *Coolmax*® fibre, showing improved effectiveness compared to commercial devices. Finally, Lee and Lee (2013) and Li et al. (2018) developed innovative high performance IEC systems applying a hydrophilic coating to heat exchanger plates.

According to the aforementioned researches (Zao et al., 2018; Wang et al., 2017; Xu et al., 2016; Xu et al., 2017; Lee and Lee, 2013), in IEC applications the study of material affinity for water is very important, in particular in terms of hydrophilicity and water retention on the plate. Droplet evaporation has been widely studied, under both constant wall heat flux and surface temperature and a reference to most significant papers can be found in Guilizzoni and Sotgia (2010). Instead, focusing the attention on recent papers specifically dealing with the effect of surface wettability, the review by Edalatpour et al. summarizes main achievements (Edalatpour et al., 2018). Lee et al. (2017) experimentally confirmed that also on transparent heaters the total evaporation time of a droplet on a hydrophilic surface is usually shorter compared to a hydrophobic surface, likely due to the long pinned phase and lower drop height that increase the average contact area between drop and surface and the drop-air interface temperature. This is consistent with a dominantly conductive heat transfer across the drop, as already assumed in pioneering works (see e.g. the works by Di Marzo and Tartarini among the already cited references in (Guilizzoni and Sotgia, 2010)) and also recently confirmed by further numerical studies (Lu et al., 2011; Yang et al., 2014) and experimental researches on engineered surfaces (Guilizzoni et al., 2018). In addition, Gao et al. (2017) confirmed that the droplet evaporation time decreases by increasing the wall heat flux and that the evaporation time on hydrophobic surfaces is higher than the one of hydrophilic surface.

The purpose of this study is to investigate the performance of an indirect evaporative cooler based on an aluminum alloy plate heat exchanger with two different surface coatings. For this objective, a system with hydrophilic coating is compared with one with a conventional epoxy lacquer. First, surface coating characteristics in terms of droplet contact angle and water retention are analyzed, then the IEC effectiveness is investigated. The experimental analysis is carried out at different operating conditions and, in particular, varying the water flowrate and nozzle position, which influence the device performance (De Antonellis et al., 2016; De Antonellis et al., 2017; Li et al., 2018).

Results provide significant information to improve the design and the management of indirect evaporative cooling systems. Although the research work is focused on data centers, the findings can be effectively used to optimize IEC systems in other applications.

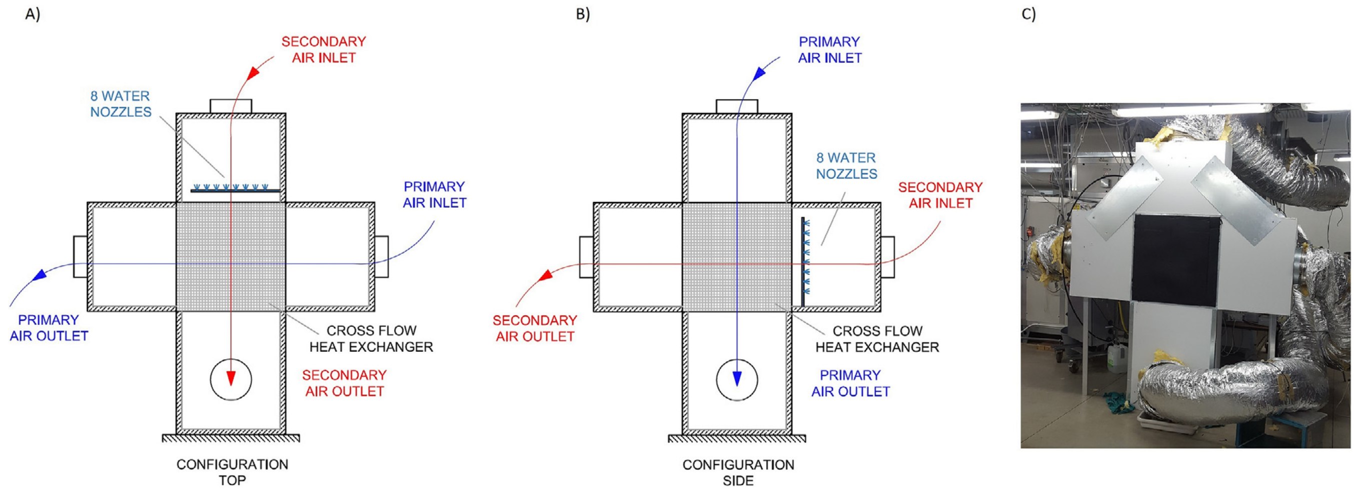

Fig. 1. Investigated IEC systems. Scheme of TOP (A) and SIDE (B) configuration and picture of the tested system (C).

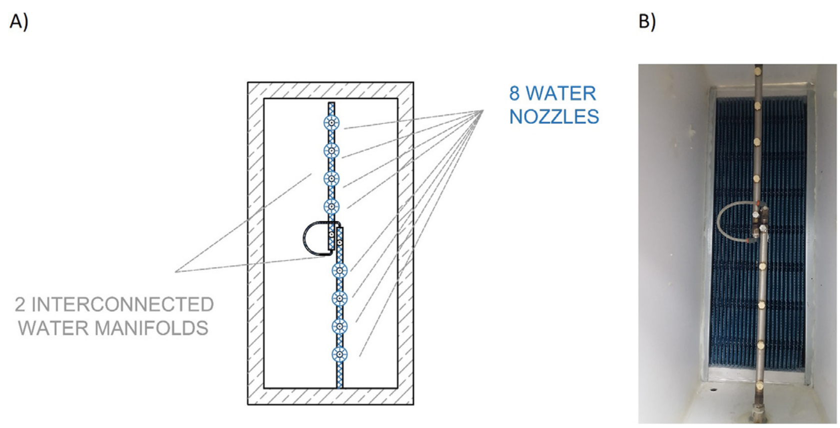

Fig. 2. Detail of secondary air inlet plenum. Scheme (A) and picture (B) of nozzles and manifolds.

2. IEC system description

The indirect evaporative cooler is a device used to cool an air stream, generally denoted as primary flow, through an air-to-air heat exchanger crossed by a secondary airflow, which is humidified with liquid water. The IEC system investigated in the present research consists of the following components: (i) a cross flow heat exchanger; (ii) eight nozzles suppling water to the secondary air stream; (iii) a pumping unit to increase water pressure. Water is appropriately supplied in the secondary air inlet plenum, in order to reach high evaporation rate and to cool the airflow both before and along the heat exchanger.

In the present research two different arrangements of the IEC system have been investigated, denoted as TOP and SIDE configuration, as shown in Fig. 1. In the first case, secondary air enters the system from the top plenum and moves downward to the bottom. Water nozzles are installed in the top plenum and the primary airflow crosses the heat exchanger in horizontal direction. Instead, in the second configuration the secondary air stream enters in a lateral plenum and leaves the system from the opposite one. Water is supplied in the secondary air inlet plenum while the primary airflow moves from the top to the bottom of the system.

In both configurations (TOP and SIDE), eight water nozzles (axial full cone type) are installed in counter current arrangement with respect to the secondary airflow. As shown in Fig. 2, nozzles are installed on two water manifolds, mounted 15 cm far from heat exchanger face, with a space step of 8 cm. Each nozzle provides 7.50 l h^{-1} when water pressure is equal to 9 bar. The length of top and side plenums is 60 cm and the length of the bottom one is equal to 100 cm.

Table 1
Main heat exchanger data (STD and HPHI).

Description	STD	HPHI
Material	Aluminium alloy	
Coating	Epoxy coating	Hydrophilic lacquer
Plates dimples	Semi spherical	
Net plates length and width - L	790 mm	
Plates number - N_{HE}	72	
Plate thickness - δ	0.15 mm	
Plate pitch - pt	3.40 mm	
Channel height - $h = pt - \delta$	3.25 mm	

Finally, IEC systems based on two different heat exchangers have been investigated. Both components are made of aluminium alloy and have the same geometry: the first one (denoted as STD) is varnished with a conventional epoxy coating while the second one (denoted as HPHI) is finished with a hydrophilic lacquer. Geometric data of both heat exchangers are reported in Table 1 and detailed characterization of the plate materials is discussed in Section 3. Note that due to the limited airflow rates that can be set through the test rig (up to 2000 m^3 h^{-1}, as discussed in Section 4), a small number of plates is adopted in order to have a representative air velocity along the heat exchanger.

Finally, combining the two configurations (TOP and SIDE) and the two heat exchangers (STD and HPHI), four different systems have been analysed:

- Configuration TOP and STD.
- Configuration TOP and HPHI.
- Configuration SIDE and STD.
- Configuration SIDE and HPHI.

Measured system performances are reported and discussed in Section 4.

3. Characterization of the heat exchanger plates material

3.1. Investigated parameters

According to the literature survey of Section 1, performance of the IEC system is primarily related to surface wettability, that in this work was consequently investigated in terms of contact angles, water retention and drop-surface interaction through photographic and high-speed video acquisitions. Static “as placed” (Tadmor and Yadav, 2008) contact angles were measured by the axisymmetric drop shape analysis (ADSA) technique in its “profile” (ADSA-P) dimensionless version (Rotenberg et al., 1983; del Rio and Neumann, 1997; Guilizzoni, 2011; Laplace, 1806; Santini et al., 2013), while high-speed videos were used to study drop-surface interactions during deposition and low speed impact.

3.2. Experimental procedure and setup

A detailed description of the theoretical aspects of ADSA-P and of the experimental setup and measurement procedures used in this work can be found in Rotenberg et al. (1983), del Rio and Neumann (1997), Guilizzoni (2011), so only a very brief summary will be given here. The ADSA-P contact angle measurement procedure is based on performing multiple integrations of the Laplace–Young equation (Laplace, 1806) in function of one or more parameters and on fitting the obtained theoretical drop profiles to the experimental drop contour. The latter is extracted from a side view photograph of a sessile drop resting on the surface of interest. Thus the values of the parameter(s) giving the “correct” drop profile can be estimated. As no closed solution is known for the drop Laplace–Young equation, numerical integration is required, that is typically performed on the axisymmetric dimensionless Laplace–Young equation written in the turning angle - arc-length coordinate system (Rotenberg et al., 1983). In this work, such equation was integrated using a basic finite difference scheme and the result fitted in a least square sense to the experimental drop contour. Once the final drop profile is calculated, the value of the turning angle at the intersection between the calculated drop profile and the baseline (horizontal line at the level of the supporting surface, manually identified by the user) is the measured contact angle. Further details about the technique, including comments about its possible issues and limitations can be found in literature (del Rio and Neumann, 1997; Guilizzoni, 2011; Laplace, 1806; Santini et al., 2013). Concerning the accuracy, tests on repeated measurements with the same drop and with repeated drop depositions allowed to estimate an overall mean absolute deviation (MAD) under 1°.

The drop-surface pictures needed for the described procedure were obtained using a customized rig. A high precision metering pump (Cole–Parmer Instrument Company, model AD74900) with suitable Hamilton syringes was used to generate drops of controlled volume (around $1.1\ 10^{-8}\ m^3 = 11\ \mu l$), while a halogen lamp equipped with a diffuser provided the light needed for the photographic and video acquisitions.

The photographs for contact angle measurement were taken using a Nikon D90 SLR digital camera equipped with a Nikkor 60 mm F2.8 Micro lens. The use of such a set-up, instead of a common commercial contact angle protractor, is aimed at reducing the typical issues affecting the sessile drop technique, i.e. focus, lighting and baseline identification problems. A side shot of the deposited drop and one of the dry surface alone are first of all acquired. Using *ad hoc* software their pixel-wise difference is calculated, segmented in drop and background and used to extract the drop contour to be fitted with the Laplace–Young equation.

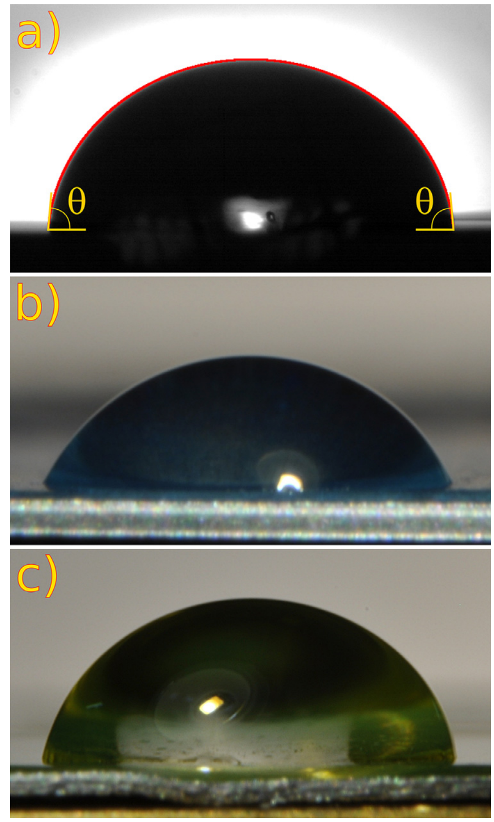

Fig. 3. Side views of sessile drops on the investigated surfaces in dry conditions, with back illumination as used for contact angle measurement and with front illumination to better evidence the drop configuration: (a) on STD surface, with fitted contour superposed to the photo and indication of the contact angles; (b) on HPHI surface; (c) on STD surface.

Dynamic drop-surface interaction was evaluated by means of high-speed videos using a Phantom Miro C110 camera, equipped with the same Nikkor 60 mm F2.8 Micro lens. Videos were acquired at a resolution of 1024×768 px, at 1200 fps with an exposure time of 820 µs.

The surfaces were investigated after cleaning with alcohol, thorough rinsing in distilled water and drying by 10 s exposure to an infrared lamp, cooling down to ambient conditions. Drop impact onto the surfaces were also analysed after immersion of the latter in distilled water followed by 10 s free de-wetting in air in vertical orientation. This allows water to leave the surface apart from the case of highly wettable surfaces on which a thin film remains. Some pictures of the heat exchanger plates after use were finally acquired, in this case using the D90 camera with a 18–105 Nikkor lens.

3.3. Experimental results

Fig. 3 shows some drop side views on the two surfaces. Panel a) is for the STD sample with back illumination as used for contact angle measurement; the fitted contour and the indication of the contact angles are superposed to the photo; panel b) and c) are with front illumination to better evidence the drop configuration, the first for the HPHI surface and the second for the STD surface.

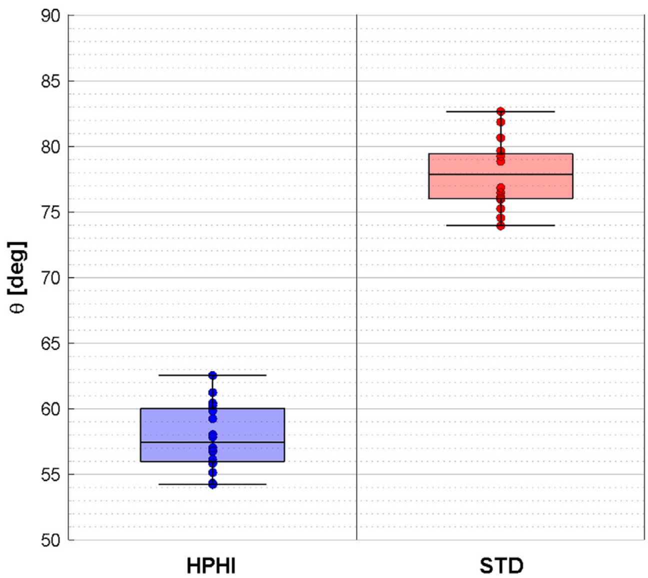

Fig. 4. Static "as placed" contact angles measured on the HPHI and STD surface samples.

A very slight "pinning on sharp edges effect", resulting in a larger apparent contact angle when the surface grooves (resulting from manufacturing) are dominantly oriented parallel to the direction of view, can be observed in some cases when drops are very gently deposed on the surface. This effect becomes absolutely negligible as soon as the drops have an even minimum impact velocity, so it is not of interest from the point of view of the real applications (also considering that in real heat exchangers plate orientation can vary). Therefore, the data in the following will be presented without distinction between groove directions.

Fig. 4 reports the results of contact angle measurement (as already said in terms of static "as placed" contact angles) on the two surfaces.

On the HPHI surface the mean contact angle is 57.8°, with a standard deviation of 2.4°; on the STD surface the mean contact angle is 77.8°, with a standard deviation of 2.5°

The measurement thus confirm that the static wettability is significantly different between the two surfaces, with the HPHI sample showing a mean contact angle 20° lower than the STD one. Related to this, and even more significant, is the different behaviour in terms of water retention: after complete coverage with water, when the sample is oriented in vertical position, the STD surface undergoes a very fast and effective autonomous de-wetting, with water immediately breaking up in isolated drops. On the contrary, the HPHI surface remains covered by a water film until the latter evaporates. In real operating conditions, the plates in the heat exchanger are continuously wet by impinging drops, so this aspect changes completely the wetting behaviour and is likely to play a fundamental role on heat exchanger performance.

Therefore, the surfaces were further analysed with respect to drop impact using high-speed cinematography. Fig. 5 shows four frame sequences on the STD and HPHI surfaces in dry conditions (denoted as dry surface) and after immersion in distilled water and positioning in vertical orientation, without any active drying to remove possible water films (denoted as wet surface).

It is evident how the impact behaviour is very similar for the dry STD and HPHI surfaces and also for the STD surface after wetting. For the latter, a small drop is visible in the pictures near to the left boundary of the surface: as already said, during de-wetting residual water assumes the shape of isolated drops. On the contrary, for the HPHI surface a film is left covering the sample and the impact behaviour is completely different.

4. IEC system performance

4.1. Test rig and experimental methodology

Two dedicated air handling units are used to control primary and secondary air conditions through heating coils and cooling coils, evaporative humidifiers and electric heaters. Primary and secondary airflow rates are controlled by variable speed fans and maximum values are 1400 $m^3\ h^{-1}$ and 2000 $m^3\ h^{-1}$. A detailed description of the test rig is reported in previous research works (De Antonellis et al., 2016; De Antonellis et al., 2017).

Each flow rate is measured through two orifice plates and piezo resistive pressure gauges (accuracy of 0.5% of reading ±1 Pa), installed according to standards (DIN EN ISO 5167-2 Standards 2003). Two coupled temperature (PT 100, accuracy of ±0.2 °C at 20 °C) and relative humidity (±1% between 0 and 90% at 20 °C) probes are installed at the inlet and outlet of each air stream. In each duct section, air states are calculated as the average of values provided by the two sensors. Finally, the water flow rate from the nozzles is measured using a turbine flow sensor (accuracy of 3% of the reading).

Each physical quantity is collected in steady state conditions at a frequency of 1 Hz (at least 300 samples). Results of each test are considered acceptable when the difference of calculated energy exchanged by primary and secondary airflows is within 5%.

The uncertainty u of directly measured quantities x_i (i.e. T, RH, p) and of calculated quantities y_i (i.e. X, ε_{wb}) is estimated in accordance with international standards (ISO IEC Guide 98-3 2008, Evaluation of measurement data 2008):

$$u_{x_i} = \pm\sqrt{u^2_{x_{i,inst}} + (t_{95}\ \sigma_{\overline{x_i}})^2} \tag{1}$$

$$u_{y_i} = \sqrt{\sum_i \left(\frac{\partial y_i}{\partial x_i} u_{x_i,inst}\right)^2 + t^2_{95}\sum_i \left(\frac{\partial y_i}{\partial x_i}\sigma_{\overline{x_i}}\right)^2} \tag{2}$$

4.2. Test conditions and performance indexes

Several tests of the IEC systems have been carried out in order to evaluate the performance of adopted configuration (TOP and SIDE) and heat exchanger plates coating (STD and HPHI). As reported in Table 2, primary and secondary air inlet states and water flow rate have been set in order to reproduce representative data center operating conditions. Inlet dry bulb air temperature and humidity ratio are set with a tolerance respectively of ± 1 °C and ± 0.5 g kg^{-1}.

In tests A, B and C, secondary air inlet dry bulb temperature, wet bulb temperature and humidity ratio have been varied two by two. In particular, in conditions A and B there is the same dry bulb temperature, in A and C the same humidity ratio and in B and C the same wet bulb temperature. Finally, in test D primary air inlet temperature is increased compared to test A while in test E the secondary air flow rate is raised with respect to test B.

In this research, performance is evaluated through the following parameters: wet bulb effectiveness ε_{wb}, fraction of evaporated water f_{eva} and dry bulb effectiveness ε_{db}, which are defined as

$$\varepsilon_{wb} = \frac{T_{p,in} - T_{p,out}}{T_{p,in} - T_{wb,s,in}} \tag{3}$$

$$f_{eva} = \frac{\dot{M}_s\ (X_{s,out} - X_{s,in})}{\dot{M}_{w,in}} \tag{4}$$

$$\varepsilon_{db} = \frac{\dot{M}_p c p_p (T_{p,in} - T_{p,out})}{(\dot{M}_{cp})_{min}(T_{p,in} - T_{s,in})} \tag{5}$$

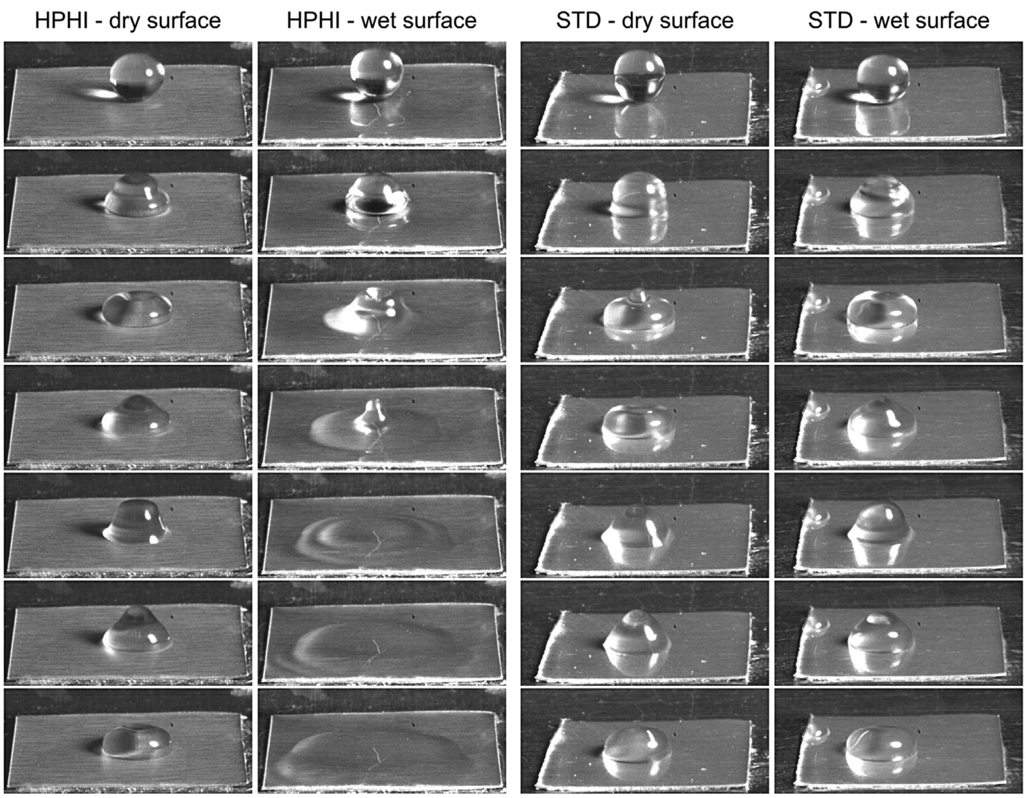

Fig. 5. Impact sequences on the STD and HPHI surfaces in dry conditions and after thorough wetting and autonomous de-wetting, but no active drying. Time interval between the following frames along each column is 3.3 ms, exposure time for each frame is 820 µs. Frames were post-processed in terms of brightness, contrast and sharpness for better visualization.

Table 2
Adopted test conditions.

Test Condition	$T_{s,in}$ [°C]	$T_{wb,s,in}$ [°C]	$X_{s,in}$ [g kg^{-1}]	$RH_{s,in}$ [%]	$\dot{Q}_s^N$ [m^3 h^{-1}]	$T_{p,in}$ [°C]	$X_{p,in}$ [g kg^{-1}]	$\dot{Q}_p^N$ [m^3 h^{-1}]	$\dot{Q}_{w,in}$ [l h^{-1}]
A	30.0	19.9	10.6	40.0	1200	35.0	10.0	1200	29–58
B	30.0	22.0	13.4	50.0	1200	35.0	10.0	1200	29–58
C	36.8	22.0	10.6	27.3	1200	35.0	10.0	1200	29–58
D	30.0	19.9	10.6	40.0	1200	40.0	10.0	1200	29–58
E	30.0	22.0	13.4	50.0	1800	35.0	10.0	1200	29–58

4.3. Experimental results

Preliminary tests have been performed to evaluate heat exchangers performance in dry conditions (no water supplied in the secondary inlet air plenum). In case of balanced airflows at $\dot{Q}_a^N = 1200$ m^3 h^{-1} and inlet temperatures equal to 20 °C and 42 °C, although the two devices have the same geometry, the measured dry bulb effectiveness was equal to 64.3% and 66.2%, respectively for HPHI and STD heat exchanger. Such variation is probably related to the manual manufacturing process of the two prototypes, which can lead to slightly different plates pitch and alignment, and, consequently, performance.

In Fig. 6 performances of the IEC system as a function of operating conditions are shown. Results are reported for TOP configuration and HPHI. A detailed analysis of ε_{wb} and f_{eva} trends for tests *A, B, C* and *E*, related to the variation of secondary air inlet conditions, has been discussed in previous works of the authors (De Antonellis et al., 2016; De Antonellis et al., 2017; Comino et al., 2018). Therefore, hereinafter only the main considerations are summarized:

- An increase in $\dot{Q}_{w,in}$ leads to an increase in the amount of evaporated water and, therefore, in ε_{wb}.
- At constant dry bulb temperature, an increase in $X_{s,in}$ leads to an increase in ε_{wb}, mainly related to the higher $T_{wb,in,s}$ (*A*–*B*).
- At constant wet bulb temperature, the higher the dry bulb temperature, the lower the heat transferred and, consequently, ε_{wb} (*B*–*C*).
- At constant inlet condition, if secondary air inlet dry bulb temperature is lower than the primary air one, an increase in the secondary airflow rate leads to an increase in ε_{wb} thanks to the higher heat transfer rate (*B*–*E*).

Finally, an increase in the primary air inlet temperature leads to a higher water evaporation rate and cooling capacity, while the wet bulb effectiveness keeps almost constant for a given water flow rate (*B*–*D*).

In next Figs. 7 and 8, performance of investigated IEC systems are compared in two representative conditions, namely *A* and *E*. Configuration TOP is analysed in Fig. 7, showing that HPHI performs better than STD. In fact, in the first case, due to the hydrophilic coating, a uniform water layer forms on heat exchanger plates, promoting water evaporation and leading to a higher cooling capacity. Differences are significant in case of limited water flow rate (around 30–35 l h^{-1}), where the wet bulb effectiveness deviation reaches 10%. In case of higher water flow rate (around 55 l h^{-1}), plates wetting of STD improves and differences in wet bulb effectiveness are reduced, even if they are still around 4–7%. Consequently, in case of TOP configuration and in the

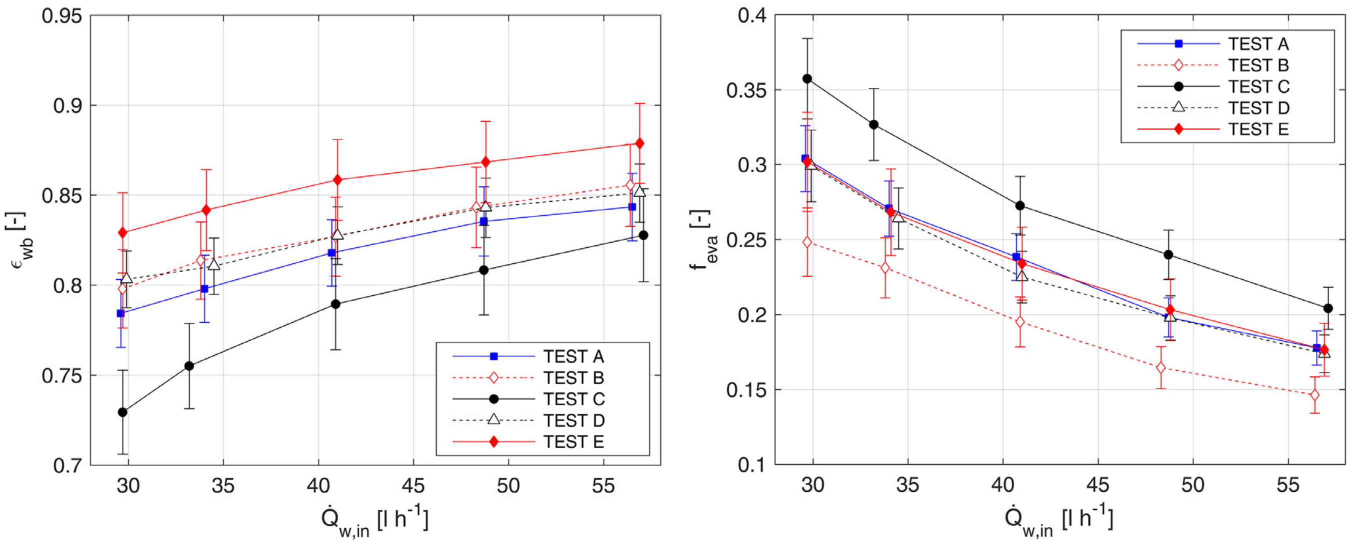

Fig. 6. TOP configuration and HPHI heat exchanger: wet bulb effectiveness and fraction of evaporated water.

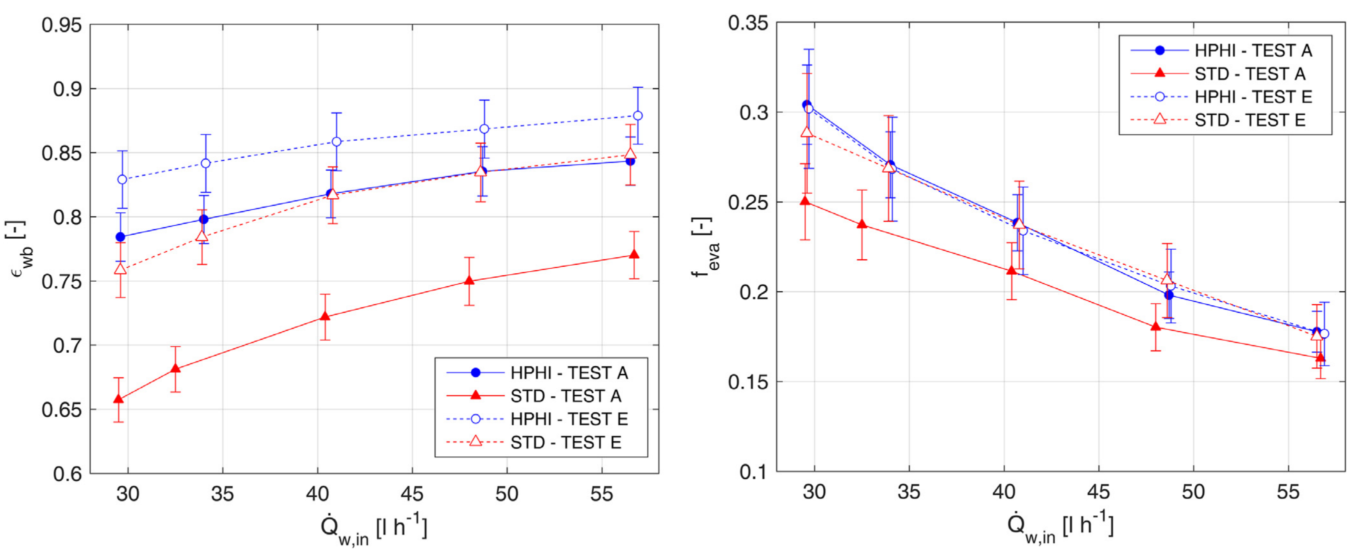

Fig. 7. TOP configuration: Comparison of wet bulb effectiveness and fraction of evaporated water between HPHI and STD heat exchanger.

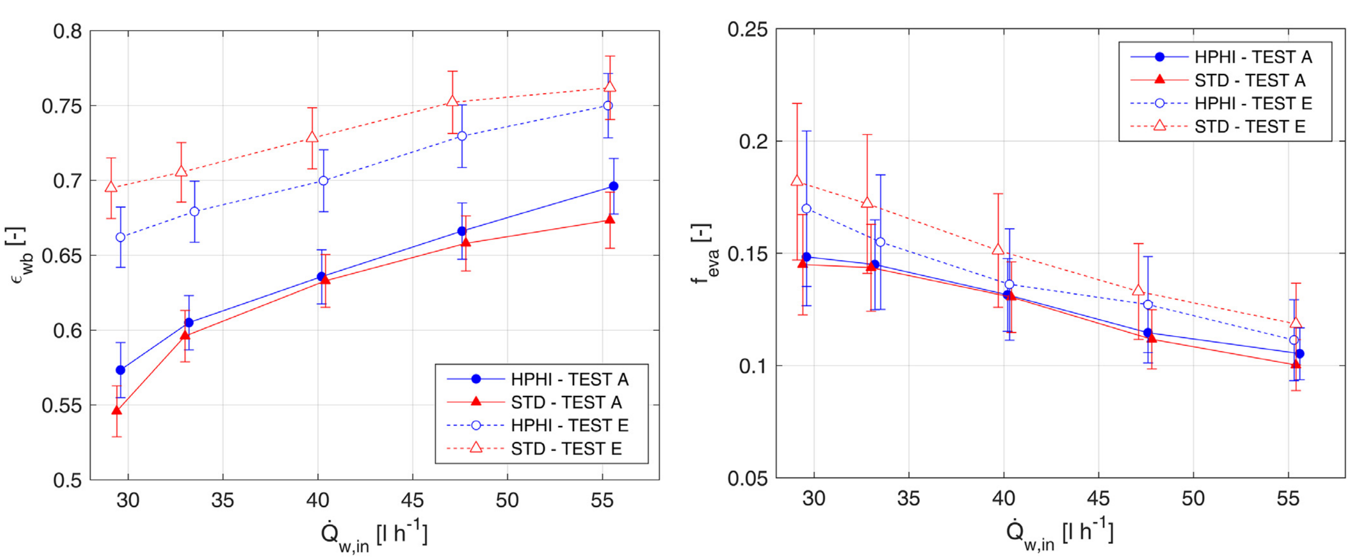

Fig. 8. SIDE configuration: Comparison of wet bulb effectiveness and fraction of evaporated water between HPHI and STD heat exchanger.

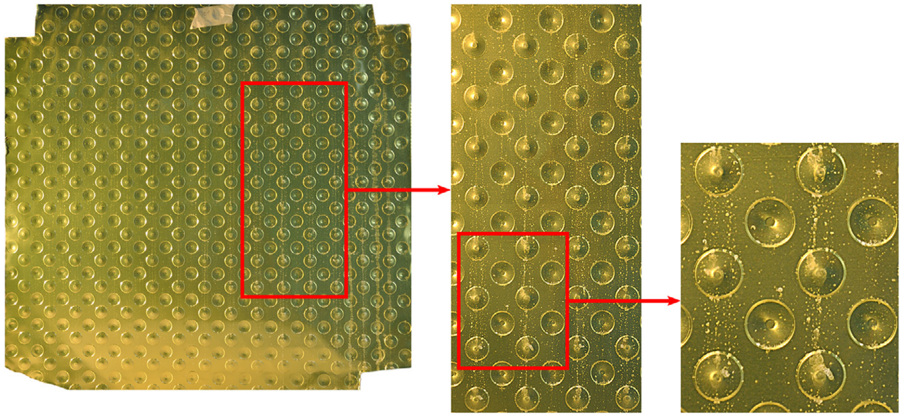

Fig. 9. Pictures of a STD plate after some weeks use with water injected from the top, evidencing the limescale deposits. Images were post-processed to increase sharpness.

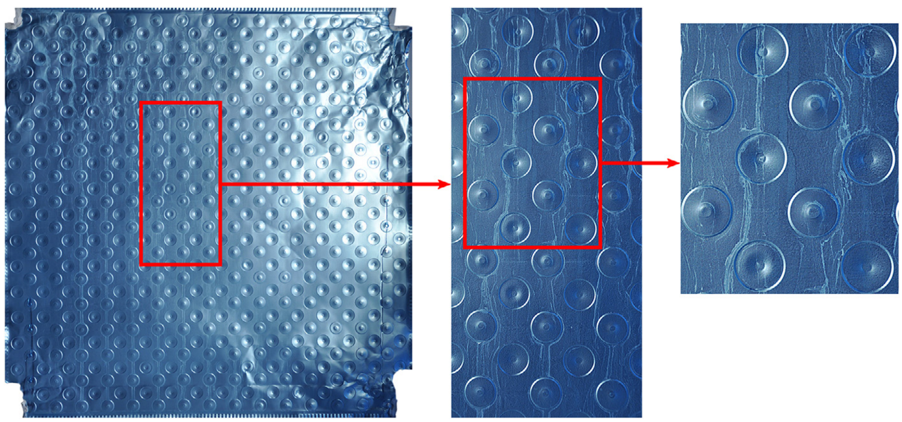

Fig. 10. Pictures of a HPHI plate after some weeks use with water injected from the top, evidencing the limescale deposits. Images were post-processed to increase sharpness.

investigated water flow conditions, the use of a heat exchanger with hydrophilic coating leads in any case to higher performance and is strongly recommended.

In Fig. 8, performance of HPHI and STD are compared in case of SIDE configuration: experimental results highlight that there is not a significant variation between the two devices and that ε_{wb} is always lower than one of TOP configuration (around 10%). In fact, in both cases plates wetting is poor because water, due to gravity force, rapidly moves downward without being able to form an effective water film along the whole horizontal extension of the heat exchanger. In case of test *E*, wet bulb effectiveness of STD is even higher than one of HPHI: such result is mainly related to the higher ε_{db} and to the experimental uncertainty. Therefore, SIDE configuration is not suggested due to poor performance compared to TOP one. In addition, if SIDE arrangement should be selected due to specific technical issues, the hydrophilic coating will not contribute to improve IEC system performance.

4.4. Plates conditions after use

To acquire further information in support of the conclusions, the two heat exchangers have been disassembled after some weeks of laboratory use, to observe the conditions of their plates. Figs. 9 and 10 show some photographs of such plates, in the case of TOP configuration. Particularly from the enlarged pictures it is evident how the limescale deposits are quite different between the two surfaces, confirming the different wetting behaviour. On the STD surface, the sediments are thicker and more localized, due to the lower hydrophilicity of the surface and its fast de-wetting, and deposited water moves along preferential paths. On the contrary, the limescale deposit in the HPHI case is much more widespread and almost all the surface is covered either by a thin layer or by a sort of “dust”.

5. Conclusions

In this work a detailed experimental analysis of two different indirect evaporative cooling (IEC) systems is carried out. In the two systems the heat exchangers plates are finished in a different way: a standard epoxy coating (STD) or a novel hydrophilic lacquer (HPHI) are adopted. The analysis is carried out through the following approach:

- Static contact angles, water retention and transient drop-surface interaction of both materials are evaluated.
- Performance of the two IEC systems is measured in different operating conditions and varying the water flowrate and nozzle position (top and side).

From the point of view of wettability, the HPHI surface is characterized by a significant increase of the hydrophilicity. The static contact angle on carefully cleaned and dried samples is lowered by around 20° and in particular the de-wetting behaviour is completely different: after contact with water, the HPHI surface remains covered by a liquid film, while an effective autonomous de-wetting happens on STD samples. This feature completely changes the spreading of drops on the surface. The different interaction with water between STD and HPHI surfaces is confirmed also by the different appearance of the limescale deposits that were observed on the plates after use. As during real operation heat exchanger plates are in continuous contact with water (in the form of mist and impinging drops), it is likely that this aspect plays a fundamental role on heat exchanger performance.

This behaviour was confirmed by tests of the indirect evaporative cooler: in case of secondary air and water flow supplied from the top of the system, performance of the device manufactured with HPHI coating is significantly higher (up to 10%). Water flows downward and, due to the improved plate's wettability, wet bulb effectiveness measured in case of HPHI material is higher, in particular at low water flow rates. More precisely, in case of test *A* ($T_{s,in} = 30\,°C$, $RH_{s,in} = 40\%$, $T_{p,in} = 35\,°C$, $\dot{Q}^N = 1200$ m^3 h^{-1}), wet bulb effectiveness values, at $\dot{Q}_{w,in}$ equal to 29 and 58 l h^{-1}, are respectively equal to:

- 78.4% and 84.4% for HPHI system.
- 65.7% and 77.1% for STD system.

Instead, in case of secondary air and water flow supplied from the side of the system, no significant differences are shown. In fact, in this case water reaches directly the bottom of the heat exchanger and it does not form a layer on heat exchanger plates, independently on superficial treatment. In case of test *A*, wet bulb effectiveness values ($\dot{Q}_{w,in}$ equal to 29 and 58 l h^{-1}) are respectively equal to:

- 57.3% and 69.6% for HPHI system.
- 54.5% and 67.3% for STD system.

Based on the experimental analysis discussed in this research, in the investigated conditions the use of a heat exchanger with hydrophilic coating arranged in the TOP configuration leads to the highest performance and, therefore, it is strongly recommended. Instead, the SIDE configuration, independently on heat exchanger coating, is not suggested due to poor performance compare to the TOP one.

Finally, although IEC performance is strongly influenced by operating conditions and system configuration and orientation, based on experimental results of this study, it is expected that HPHI coating can improve performance of a generic IEC device, in particular in case of low and vertical (downstream) water flow.

Acknowledgments

The authors acknowledge Recuperator S.p.A. personnel, in particular Mr Leone and Mr Bawa, for the technical and economic support provided during the research study.

References

ASHRAE. 2008. Thermal Guidelines for Data Processing Environments, 2nd edition

Chengqin, R., Hongxing, Y., 2006. An analytical model for the heat and mass transfer processes in indirect evaporative cooling with parallel/counter flow configurations. Int. J. Heat Mass Transf. 49 (3), 617–627.

Chua, K.J., Xu, J., Cui, X., Ng, K.C., Islam, M.R., 2016. Numerical heat and mass transfer analysis of a cross-flow indirect evaporative cooler with plates and flat tubes. Heat Mass Transf./Waerme- und Stoffuebertragung 52 (9), 1765–1777.

Chung, J.D., Lee, D.Y., 2011. Contributions of system components and operating conditions to the performance of desiccant cooling systems. Int. J. Refrig. 34, 922–927. doi:10.1016/j.ijrefrig.2011.03.003.

Comino, F., Milani, S., De Antonellis, S., Joppolo, C.M., Ruiz de Adana, M., 2018. Simplified performance correlation of an indirect evaporative cooling system: development and validation. Int. J. Refrig. 88, 307–317 ISSN 0140-7007.

De Antonellis, S., Joppolo, C.M., Liberati, P., Milani, S., Molinaroli, L., 2016. Experimental analysis of a cross flow indirect evaporative cooling system. Energy Build. 121, 130–138 ISSN 0378-7788. doi:10.1016/j.enbuild.2016.03.076.

De Antonellis, S., Joppolo, C.M., Liberati, P., Milani, S., Romano, F., 2017. Modeling and experimental study of an indirect evaporative cooler. Energy Build. 142, 147–157.

del Rio, O.I., Neumann, A.W., 1997. Axisymmetric drop shape analysis: computational methods for the measurement of interfacial properties from the shape and dimensions of pendant and sessile drops. J. Colloid Interf. Sci. 196, 136–147. doi:10.1006/jcis.1997.5214.

DIN EN ISO 5167-2 Standards, Measurement of fluid flow by means of pressure differential devices inserted in circular cross-section conduits running full—Part 2: orifice plates (ISO 5167-2:2003). International Organization for Standardization, Geneva, Switzerland.

Duan, Z., Zhan, C., Zhang, X., Mustafa, M., Zhao, X., Alimohammadisagvand, B., Hasan, A., 2012. Indirect evaporative cooling: past, present and future potentials. Renew. Sustain. Energy Rev. 16 (9), 6823–6850 ISSN 1364-0321.

Edalatpour, M., Liu, L., Jacobi, A.M., Eid, K.F., Sommers, A.D., 2018. Managing water on heat transfer surfaces: a critical review of techniques to modify surface wettability for application with condensation and evaporation. Appl. Energy 222 (15), 967–992.

Evaluation of measurement data – Guide to the expression of uncertainty in measurement JCGM 100:2008 (GUM 1995 with minor corrections).

Gao, M., Kong, P., Zhang, L.X., Liu, J.N., 2017. An experimental investigation of sessile droplets evaporation on hydrophilic and hydrophobic heating surface with constant heat flux. Int. Commun. Heat Mass Transf. 88, 262–268.

Goldsworthy, M., White, S., 2011. Optimisation of a desiccant cooling system design with indirect evaporative cooler. Int. J. Refrig. 34, 148–158. doi:10.1016/j.ijrefrig.2010.07.005.

Guilizzoni, M., 2011. Drop shape visualization and contact angle measurement on curved surfaces. J. Colloid Interf. Sci. 364 (1), 230–236. doi:10.1016/j.jcis.2011.08.019.

Guilizzoni, M., Sotgia, G., 2010. Experimental analysis on the shape and evaporation of water drops on high effusivity, microfinned surfaces. Exp. Therm. Fluid Sci. 34, 93–103. doi:10.1016/j.expthermflusci.2009.09.006.

Guilizzoni, M., Sotgia, G., González-Esteve, A., 2018. A correlation for dropwise cooling on metallic microfin surfaces. Exp. Therm. Fluid Sci. 97, 70–78. doi:10.1016/j.expthermflusci.2018.04.001.

Guo, X.C., Zhao, T.S., 1998. A parametric study of an indirect evaporative air cooler. Int. Commun. Heat Mass Transf. 25 (2), 217–226.

ISO IEC Guide 98-3, 2008. Uncertainty of Measurement—Part 3: Guide to Expression of Uncertainty in Measurement. International Organization for Standardization, ISO IEC Guide 98-3, Geneva Switzerland.

Koomey, J., 2011. Growth in Data Center Electricity Use 2005 to 2010. Analytics Press, Oakland, CA.

Laplace, P.-S., 1806. Théorie De L'action Capillaire - Supplément au Dixième Livre Du Traité De Mécanique Céleste. Courcier, Paris.

Lee, J., Lee, D.-Y., 2013. Experimental study of a counter flow regenerative evaporative cooler with finned channels. Int. J. Heat Mass Transf. 65, 173–179 ISSN 0017-9310.

Lee, S., Kim, D.I., Kim, Y.Y., Park, S.-E., Choi, G., Kim, Y., Kim, H.-J., 2017. Droplet evaporation characteristics on transparent heaters with different wettabilities. Royal Soc. Chem. Adv. 7, 45274–45279.

Li, W.-Y., Li, Y.-C., Zeng, L.-Y., Lu, J., 2018. Comparative study of vertical and horizontal indirect evaporative cooling heat recovery exchangers. Int. J. Heat Mass Transf. 124, 1245–1261 ISSN 0017-9310.

Lu, G., Duan, Y.-Y., Wang, X.-D., Lee, D.-J., 2011. Internal flow in evaporating droplet on heated solid surface. Int. J. Heat Mass Transf. 54, 4437–4447. doi:10.1016/j.ijheatmasstransfer.2011.04.039.

Najjar, Y.S.H., Abubaker, A.M., 2015. Indirect evaporative combined inlet air cooling with gas turbines for green power technology. Int. J. Refrig. 59, 235–250 ISSN 0140-7007.

Rotenberg, Y., Boruvka, L., Neumann, A.W., 1983. Determination of surface tension and contact angle from the shapes of axisymmetric fluid interfaces. J. Colloid Interface Sci. 93, 169–183. doi:10.1016/0021-9797(83)90396-X.

Salim, M., Tozer, R., 2010. Data centers' energy auditing and benchmarking-progress update. ASHRAE Trans. 116, 109–117.

Santini, M., Guilizzoni, M., Fest-Santini, S., 2013. X-ray computed microtomography for drop shape analysis and contact angle measurement. J. Colloid Interface Sci 409, 204–210. doi:10.1016/j.jcis.2013.06.036.

Tadmor, R., Yadav, P.S., 2008. As-placed contact angles for sessile drops. J. Colloid Interface Sci. 317, 241–246. doi:10.1016/j.jcis.2007.09.029.

Van Heddeghem, W., Lambert, S., Lannoo, B., Colle, D., Pickavet, M., Demeester, P., 2014. Trends in worldwide ICT electricity consumption from 2007 to 2012. Comput. Commun. 50, 64–76.

Wang, F., Sun, T., Huang, X., Chen, Y., Yang, H., 2017. Experimental research on a novel porous ceramic tube type indirect evaporative cooler. Appl. Therm. Eng. 125, 1191–1199.

Xu, P., Ma, X., Zhao, X., Fancey, K., 2017. Experimental investigation of a super performance dew point air cooler. Appl. Energy 203, 761–777 ISSN 0306-2619.

Xu, P., Ma, X., Zhao, X., Fancey, K.S., 2016. Experimental investigation on performance of fabrics for indirect evaporative cooling applications. Build. Environ. 110, 104–114 ISSN 0360-1323.

Yang, K., Hong, F., Cheng, P., 2014. A fully coupled numerical simulation of sessile droplet evaporation using Arbitrary Lagrangian–Eulerian formulation. Int. J. Heat Mass Transfer 70, 409–420. doi:10.1016/j.ijheatmasstransfer.2013.11.017.

Zao, X., Liu, S., Riffat, S.B., 2018. Comparative study of heat and mass exchanging materials for indirect evaporative cooling systems. Build. Environ. 43 (11), 1902–1911.